Asia-Pacific Journal of Atmospheric Sciences
https://doi.org/10.1007/s13143-019-00157-2

Online ISSN 1976-7951
Print ISSN 1976-7633

ORIGINAL ARTICLE

Impact of Spring AAO on Summertime Precipitation in the North China Part: Observational Analysis

Zhengxuan Yuan[1] · Jun Qin[1] · Shuanglin Li[1] · Sijing Huang[1] · Yassin Mbululo[1,2]

Received: 18 March 2019 / Revised: 29 September 2019 / Accepted: 27 October 2019

Abstract
By using the 160 stations monthly precipitation data and NOAA-ESRL reanalysis data, the effect of spring Antarctic Oscillation (AAO) on Summer Precipitation in North China (SPNC) is studied. The analysis results show that the positive phase of March AAO leads the easterly-southerly and ascend anomalies in the southern part of North China by affecting zonal wind, and meridional circulation in the Northern Hemisphere (NH) late summer, results in more SPNC. Key regions of Antarctic sea-ice may store preceding March AAO signal which is cross-seasonal sustained by the heat exchanging with underlying surface, and the Summer Antarctic Sea-ice Index (SSI) is defined. The upward and poleward propagations of the planetary wave are enhanced in the Southern Hemisphere (SH) high latitude, and there are significant anomalous variabilities of PSI over SH low latitude, high latitude and polar regions in the high SSI years and vice versa. The wave-current interaction weakens the descending motion over the Antarctic, strengthens the circumpolar westerlies and deepens the SH polar vortex (AAO positive phase) in the high SSI years and vice versa. The results of observation and CAM5 show that SSI is positively correlated with indices of Quasi-Biennial Oscillation (QBOI). In QBO westerly phase, the SPNC anomaly in the high SSI years shows out of phase with that in the low SSI years. In the low SSI years, Rossby wave has the characteristics of anomalous southward propagation which corresponds to the abnormal weakening of ascend motion (the decrease of precipitation) over North China. Accompanied with a significant PSI anomaly, there exists a region of weak to strong wave energy over North China which is regarded as the source region of wave energy in both high and low SSI years of QBO westerly phase. But in QBO easterly phase, SPNC anomaly is not significant. QBO may be a bridge that connecting the signals of zonal wind anomalies in the stratosphere of the SH and the NH.

Keywords AAO · Sea ice · Stratosphere · Precipitation

1 Introduction

The Antarctic Oscillation (AAO) which is also called Southern Annual Mode (SAM), is the dominant mode of variability in Southern Hemisphere (SH). North Hemisphere (NH) climate is characterized by the leading AAO (Silvestri and Gabriel, 2003; Fan and Wang 2006; Song and Zhou 2014). AAO also influences regional weather in China. For instance, when the magnitude of AAO increases (decreases) in February, the precipitation in North China increases (decreases). Similarly, when it increases in Spring, precipitation represents a dipole structure of increasing in North and decreasing in South (Qin et al. 2004; Fan and Wang 2007). Spring AAO often has an adjustment for East Asia Summer Monsoon (EASM) by equatorial flow from Australian and Maskerlin high pressure or West Atlantic which could induce the wave train of JP (Japan-Pacific) (Nitta 1987; Huang and Li, 1987; Xue et al. 2003; Gao et al. 2003; Wu et al. 2007; Lin et al. 2013). It can also change significantly the summer synoptic circulations as well as local meteorology in China (Fan and Wang, 2004). Note that, variabilities in precipitation in China are often attributed to ascending motion, east-southerly and west-southerly, followed by the influence of AAO. More importantly, precipitation always reaches the maximum level in summer over most of East China regions, and it could have vital connection with drought and flood

Responsible Editor: Kyong-Hwan Seo.

✉ Jun Qin
qinjun@cug.edu.cn

[1] School of environmental studies, China University of Geosciences (Wuhan), Hubei 430074, China

[2] Department of Geography and Environmental Studies, Sokoine University of Agriculture, Morogoro, Tanzania

Published online: 02 January 2020

disasters in this season, as well as in North China (Qin et al. 2005; Fan 2006).

North China precipitation has attracted much attention of meteorological experts (Yang et al. 2005; Tu et al. 2010; Shao et al. 2018; Sun et al. 2018). In general, the rainy season in North China is characterized by interannual variations, usually beginning in early July and ending in late August or early September (Li and Guo 2015). To our knowledge, only few studies have analyzed the relationships between AAO and North China precipitation. In general, AAO influences NH climate (Zhou and Yu 2004; Fan and Wang 2007; Song et al. 2009; Wu 2010; Liu et al. 2014). Study by Song et al. (2009) investigated the signatures of AAO in the upper troposphere of NH and found that during boreal winter, a positive (negative) phase of the AAO was associated with anomalous easterlies (westerlies) in middle-low latitudes (30–40°N) and anomalous westerlies (easterlies) in middle-high latitudes (45–65°N) of the upper troposphere for about 25–40 days later. Tropical zonal wind anomalies can trigger a Pacific/North American teleconnection patterns (PNA) like quasi-stationary Rossby waves that propagate into the Northern Hemisphere and gradually evolve into patterns which resemble North Atlantic teleconnection patterns. Furthermore, these quasi-stationary Rossby waves might give rise to anomalous eddy momentum flux convergence and divergence to accelerate anomalous zonal winds in the NH. Using a combination of observations and modeling simulations, Zhou and Yu (2004) pointed out that the reproducibility is greater during Austral summer than winter, and the source of much of the reproducibility is tropical Pacific SST. The warmer equatorial Pacific event corresponds to a negative phase of AAO in Austral summer. Liu et al. (2014) suggested that, the boreal Autumn SAM was associated with changes in surface subpolar westerlies, which influenced the surface heat exchange and drove the meridional oceanic Ekman flow which redistributed heat near the surface. A 'sea-air coupled bridge' allows the influence of the boreal Autumn SAM to persist to the following season and affects the NH climate.

In this study, we demonstrate that Summer Precipitation in North China (SPNC) is more closely related to Antarctic sea ice concentration (ASIC). The AAO is likely to have effects on the SPNC through altering regional meteorology and synoptic circulations. Previous studies have emphasized the influence of sea ice to climate of China and global (Bian and Lin 2008; Amita et al. 2009; Bian et al. 2010; Wu and Zhang 2011; Screen 2013; Bintanja and Selten, 2014). Bian and Lin (2008) defined an index of Antarctic sea-ice oscillation with a seesaw pattern and presented the relationship with summer precipitation in China. Their result showed that the winter index had significant correlation with abnormal summer (June–August) precipitation in China and the area of significant correlation represented a dipole structure with positive area at the southern part and negative at the northern part. Screen (2013) suggested that diminished Arctic sea ice associated with recent wet summers in Europe. These relationships suggest the existence of a link between spring AAO, polar sea ice and summer precipitation in China.

Based on the above analysis, a question arises: Does ASIC play a role of storage for AAO? If so, is there any other approach to the influence of the AAO on following SPNC except traditional tunnel of the Indian Ocean and Pacific Ocean? To solve this problem, we will calculate the index of important area of Antarctic sea ice which could be the storage of previous signals of AAO for further identification. We analyze the mechanism by using boreal Summer Antarctic Sea-ice Index (SSI) and Quasi-biennial oscillations in the equatorial stratosphere (QBO). We try to figure out an ice-stratosphere bridge between previous AAO and following SPNC.

2 Materials & Methods

We obtained the 1979–2017 monthly mean precipitation data from NOAA PREC/L (https://www.esrl.noaa.gov/psd/data/gridded/data.precl.html). We also used the precipitation data from 160 meteorological stations provided by CMA (China Meteorological Administration). The meteorological data used in this study consist of sea level pressure (SLP), geopotential height (GPH), vertical velocity (omega), wind speed and heat flux were obtained from the National Centers for Environmental Prediction Reanalysis 1 with a 2.5° × 2.5° grid resolution.

The indices of AAO, Nino3.4 and Quasi-Biennial Oscillation (QBO) were obtained from NOAA (https://www.esrl.noaa.gov/psd/data/climateindices/list/). The AAO index (AAOI) is defined as the first leading mode from the EOF analysis of monthly mean GPH anomalies at 700 hPa (SH) (Thompson and Wallace, 2000). The QBO index (QBOI) is defined by averaging the zonal mean zonal wind speed ([U], in which U denotes zonal wind speed and square brackets denote zonal mean) over equator at 30 hPa. We obtained the 1979–2014 monthly mean sea ice concentration data from NOAA (https://www.esrl.noaa.gov/psd/data/gridded/data.20thC_ReanV2c.html). By using linear detrend method (the ENSO index equals Nino3.4 index), the influence of ENSO is eliminated from AAOI and other indices which are defined in the following content. The index of SPNC (SPNCI) is defined by averaging the precipitation in the southern part of North China ([112.5–118.5°E, 35–40°N]).

The classical statistical methods used in following content include the calculation of correlation coefficients, slopes and significance test (student-t test, p value test). The slopes in the following content, for example, there is a linear regression relationship between the normalized series of sample X and series of sample Y: $Y = AX + B$, in which A represents the

slope, indicating that when normalized X increases by 1 unit as an independent variable, the dependent variable Y will increases by A.

We examined the potential atmospheric linkage of underlying surface layer by using the maximum covariance analysis (MCA, also called Singular Value Decomposition - SVD). The MCA analysis is an excellent climate analysis method which has been widely used for catching the potential links between atmospheric signals and external forcing such as sea surface temperature and sea ice (Wu and Zhang, 2011; Hu et al. 2016). The MCA patterns describe the spatial structure of each respective field (left field and right field). And the corresponding squared singular values represent the covariance fraction (CF), which in turn reflects the relative importance of each MCA mode in relation to the total covariance of two fields.

Atmospheric signals are transmitted from troposphere to stratosphere through wave-current interaction. A wave action vector describing the propagation of 3D planetary waves is used to diagnose the cause of circulation anomalies. Plumb flux (F_s) was derived by Plumb (1985) and further used in the study of Tan et al. (2010) and Yang et al. (2015). Furthermore, Takaya and Nakamura (2001) updated the F_s as the T-N wave flux (Denoted as W) and the T-N equation is shown (Eq. 1). The T-N flux is a kind of 3D wave activity flux that is calculated in the quasi-geostrophic framework, which can identify the origin and propagation of the energy of the Rossby wave like perturbation (Hsu and Lin 2007; He et al. 2018)

$$W=\frac{p_0\cos\varphi}{2|U|}\begin{pmatrix}\frac{U}{a^2\cos^2\varphi}\left[\left(\frac{\partial\psi'}{\partial\lambda}\right)^2-\psi'\frac{\partial^2\psi'}{\partial\lambda^2}\right]+\frac{V}{a^2\cos\varphi}\left[\frac{\partial\psi'}{\partial\lambda}\frac{\partial\psi'}{\partial\varphi}-\psi'\frac{\partial^2\psi'}{\partial\lambda\partial\varphi}\right]\\ \frac{U}{a^2\cos\varphi}\left[\frac{\partial\psi'}{\partial\lambda}\frac{\partial\psi'}{\partial\varphi}-\psi'\frac{\partial^2\psi'}{\partial\lambda\partial\varphi}\right]+\frac{V}{a^2}\left[\left(\frac{\partial\psi'}{\partial\varphi}\right)^2-\psi'\frac{\partial^2\psi'}{\partial\varphi^2}\right]\\ \frac{f_0^2}{N^2}\left\{\frac{U}{a\cos\varphi}\left[\frac{\partial\psi'}{\partial\lambda}\frac{\partial\psi'}{\partial z}-\psi'\frac{\partial^2\psi'}{\partial\lambda\partial z}\right]+\frac{V}{a}\left[\frac{\partial\psi'}{\partial\varphi}\frac{\partial\psi'}{\partial z}-\psi'\frac{\partial^2\psi'}{\partial\varphi\partial z}\right]\right\}\end{pmatrix}+C_U \quad (1)$$

In Eq. (1), a represents the earth radius. $p_0=p/1000$; U represents the steady zonally inhomogeneous basic flow, while ψ' represents the perturbation stream function (PSI). $N^2=(R_a{p_0}^{\kappa}/H)(\partial\theta/\partial z)$ is the buoyancy frequency squared where $z=-H\ln p$, H represents constant scale height, θ denotes potential temperature, R_a the gas constant of dry air, $\kappa=R/c_p$, in this manuscript, $\kappa=0.286$. In computation, we assumed the wave is stationary, so the C_U in Eq. (1) is zero (0).

It should be emphasized that the time series in following content is generally from 1979 to 2017, but the time series in sea-ice-related analysis is from 1979 to 2014.

3 Results & Discussions

3.1 Impact of AAO on North China Precipitation

As a first step, we calculate the correlations between February and May AAO Index and SPNC (average of precipitation in July and August) from 1979 to 2017 (Figures not show). It is found that March AAOI (M-AAOI denotes March AAOI from here to the following content) is highly positive correlated with SPNC, as shown in Fig. 1. Figure 1c suggests that, SPNC increases by 60~120 mm when M-AAOI increases from lower state to higher state, and vice versa. Corroborated results to this have been reported by Qin et al. (2005), as they found Spring AAO was highly positive related to SPNC.

For the persistence of March AAO signals, Fig. 2a to c show the correlations between M-AAOI and geopotential height (GPH). It is obviously that the positive phase of March AAO persists to the following summer, especially on July to August. In the summer, there are significant positive anomalies in the mid-high latitudes of the NH, while the cross-equatorial effect is more obvious at 850 hPa (Fig. 2c). Figure 3a to c, which represent the relationship between M-AAOI and zonal wind, show positive phase of corresponding AAO. It is clear that, the positive phase of March AAO could be well reflected in following summer, and extends to stratosphere. In the summer, the zonal wind, in the latitude from 30°N to 40°N, represents negative anomalies while the area that reaches the statistically significant appears in June. It is noteworthy that the summer zonal wind shows a significant negative anomaly (easterly anomaly) at 100 hPa over the equator. Two obvious AAO signs, the deepening of polar vortex and the enhancement of the SH circumpolar westerly, persist from March to late summer. Such signs highlight the cross-seasonal feature of AAO.

The effect of AAO on the NH meridional circulation has been mentioned many times in the past studies (Song et al. 2009; Liu et al. 2014). Figure 4a shows the composite difference of meridional circulation between high and low M-AAOI

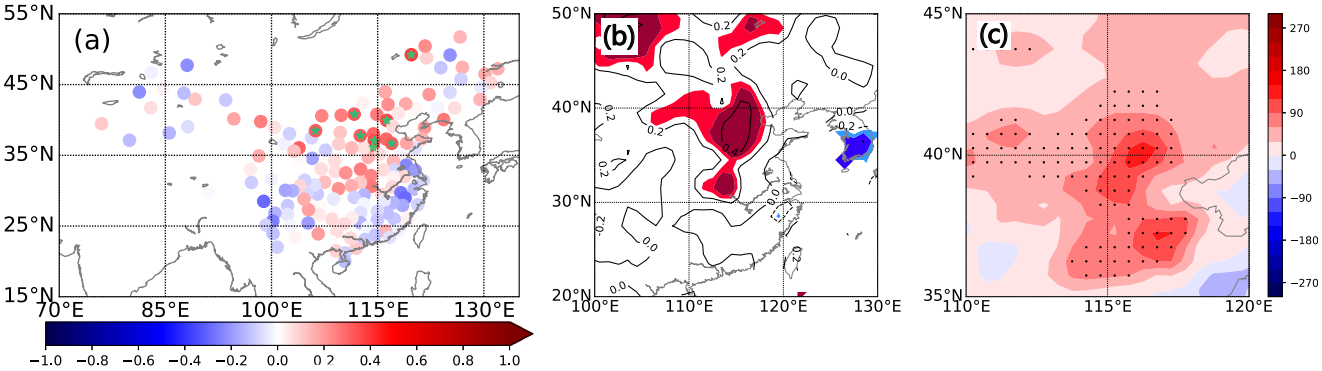

Fig. 1 (a) Scatters map of correlation between M-AAOI and summer precipitation in China, totally 160 stations (Green * mark: reaches statistically significant ($p \leq 0.05$)) (b) Correlation between summer precipitation anomaly in China and M-AAOI from the year 1979 to 2017 (Contour interval: 0.2); dark shaded: reaches statistically significant $p \leq 0.05$, light shaded: $p \leq 0.1$, red color represents positive while the blue color represents negative) (c) Composite difference of SPNC between high and low M-AAOI years (The black scattered regions denote the significant anomalies reach the 90% confident level for student-t test, unit: mm)

(0.5 times standard deviation of standardized M-AAOI) years. Figure 4b shows the composite difference of meridional circulation between high and low SPNCI (0.5 times standard deviation of standardized SPNCI) years. The shading of these figures represents the climatology average of summer (July–August: JA) vertical velocity (omega). Figures show the ascending motion from equator to 40°N and descending motion from equator to nearly 40°S. It could be concluded that significant ascending and southerly anomalies are exhibited over the 35°N to 40°N in high M-AAOI years. That is, the higher rate of SPNC is associated with the simultaneous overlying ascending-southerly anomalies which are partially attributed to preceding higher phase of March AAO.

Over East Asia, there exhibits a dipole structure which will be discussed in subsection 3.3. Generally, mode of March AAO is obviously reflected by zonal wind at the same period and in the following summer. Figure 5a shows the vertical profile of correlation between M-AAOI and JA zonal mean (110–120°E) zonal wind, exhibits AAO like structure in the SH and dipole structure from 20°N to 60°N with the center at about 200 hPa (Height of boreal summer westerly jet). It is notable that positive anomalies also occur in the equatorial stratosphere. The dipole structure for JA zonal wind anomalies is also statistically related with SPNCI (Fig. 5b), for the fact that northward westerly jet is a necessary condition for SPNC (Zhao et al. 2017).

It is worth to note that AAO signals can be stored in the ocean through 'sea-air' interaction and can last for several months. Through above analysis, we found that March AAO has significant impact on following summer NH circulation. So how does AAO in March affect the climate in late summer? Previous studies had pointed out that 'sea-air bridge' could be the storage mechanism of early AAO and late signals of early AAO (Ho et al. 2005; Choi et al. 2014). Similarly, this section presents the 'ice-air bridge' which means that sea ice is sensitive to dynamic and thermodynamic forcing overlying atmosphere and underlying ocean, acts as the storage of preceding atmospheric signals. Study by Wu and Zhang (2011) analyzed the relationship between the AAO, heat flux and sea ice concentration, and found out a significant covariance between the winter sea ice concentration anomalies and the late springtime atmospheric circulation. The atmospheric signals persisted up to four months through heat exchanging with underlying sea ice. Figure 6a to e show the leading MCA mode between JA Antarctic sea ice concentration (JA-ASIC) and 700 hPa-GPH (H700) south of 20°S from MA to JA for 1979 to 2014 (We use geopotential height at 700 hPa because the definition of AAOI from the study by Thompson and

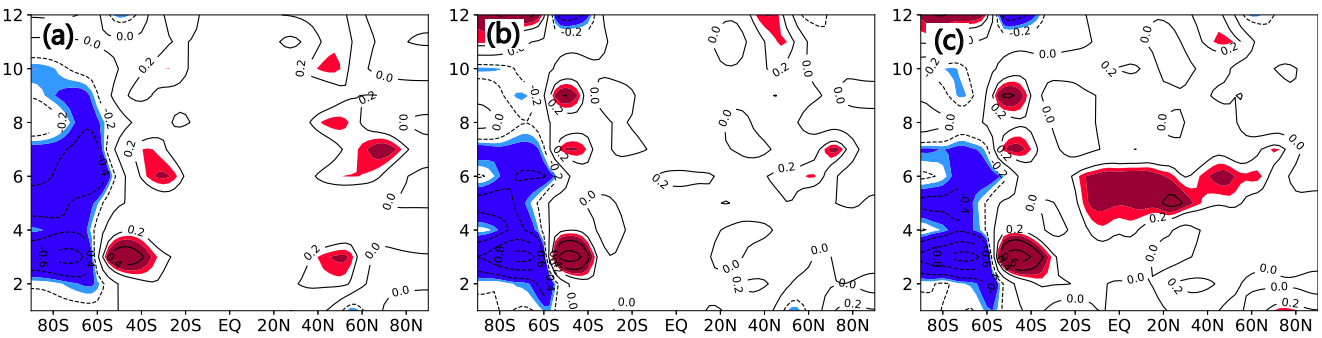

Fig. 2 Correlations between M-AAOI and GPH (a) 100 hPa (b) 500 hPa (c) 850 hPa (x-axis represents latitude, y-axis represents month, shaded: same as Fig. 1b)

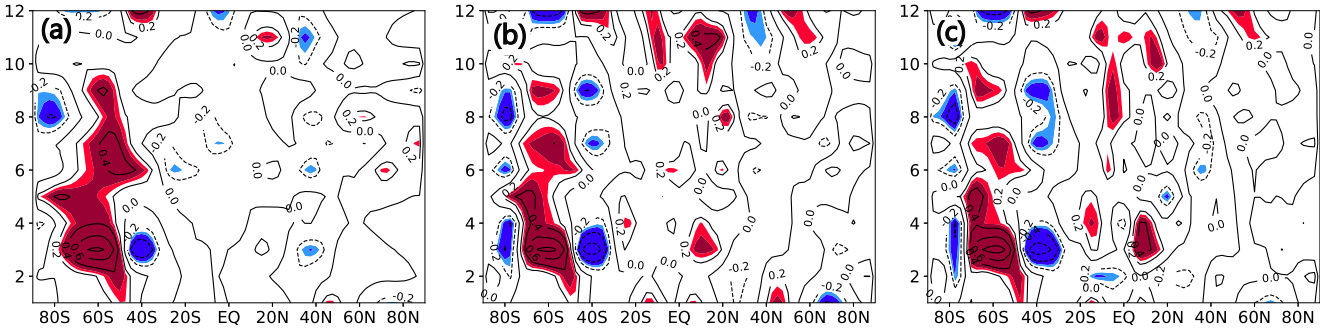

Fig. 3 Correlations between M-AAOI and [U] (a) 100 hPa (b) 500 hPa (c) 850 hPa (same as Fig. 2)

Wallace, 2000). Each figure contains two subfigures, the one on the left side is the heterogeneous correlation map of left field, which means the correlation coefficients between time series of right field (H700) and special mode of left field (JA-ASIC). The one on the right side is the heterogeneous correlation map of right field. Each title of figures contains the name of each pattern, CF value and correlation coefficient between two time series of each pattern (CR). It could be seen from Fig. 6 that March AAO positive structure has maintained the change of ASIC which generally represents a dipole pattern with negative anomalies in the west and positive anomalies in the east from 40°W eastward to 40°E. However, the heterogeneous correlation map of MA-ASIC shows only significant near the land boundary of Antarctic, which might be attributed to the lack of Antarctic sea ice in boreal spring (austral autumn). The heat exchange might be active between Antarctic atmosphere and underlying ocean (reflected by sea surface temperature) in boreal spring. With the increase of ASIC, the relationship between March AAO and ASIC becomes more significant, and the relative higher values of CF and CR appear from June to August. Such persistence of atmospheric signals by heat exchanging with underlying surface is still suitable from boreal spring to late summer.

Here, we calculate the correlations between March AAO and JA-ASIC, as shown in Fig. 7a. Based on Fig. 6, 7a and correlation between SPNCI and JA-ASIC (figure not shown), we choose the significant correlation regions of JA-ASIC (KA1[60–65°S, 20–30°E] and KA2[54–56°S, 5–40°W]) as the key regions. The Summer Antarctic Index (SSI) is defined by the difference of area-averaged JA-ASIC between KA1 and KA2. Note that, the boreal spring ASIC is very low, so we calculate the correlation between M-AAOI and heat flux from JF to JA to clarify the relationship between March AAO and underlying surface. The robustness of heat exchange between March AAO and underlying surface will be ensured.

The correlation coefficients between M-AAOI, SSI and HFI (Index of heat flux, calculation method is same as SSI) from JF to JA are showed in Fig. 7b. Note that, the JA-HFI is out of phase with MA-HFI and May–June (MJ)-HFI, shows the progress of atmospheric signals storing and releasing. It could be said that the signals of March AAO persist to late July–August by the surface heat exchange between Antarctic sea ice, the Southern Ocean and overlying atmosphere. The correlation coefficient (r) between the SPNCI and SSI was equal to 0.35, statistically significant $p \leq 0.05$. Meanwhile, the correlation between the northern part of North China

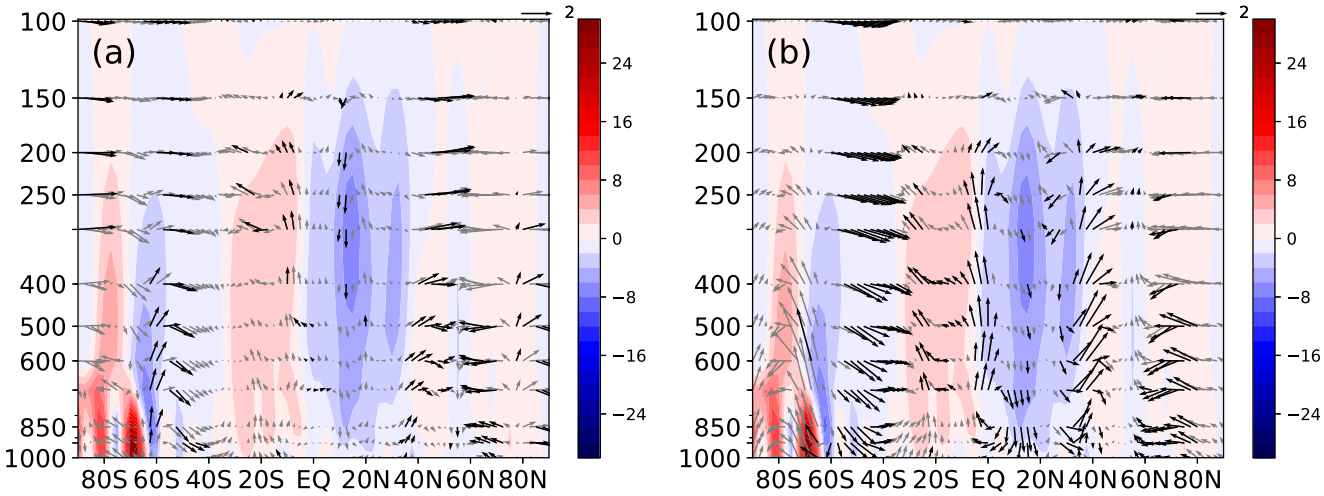

Fig. 4 Composite difference of JA meridional circulation between high and low (a) M-AAOI years (b) SPNCI (Shaded: Climatology vertical velocity - omega, the unit of omega: 1% Pa/s; Black vector: composite difference reaches the 90% confident level for student-t test)

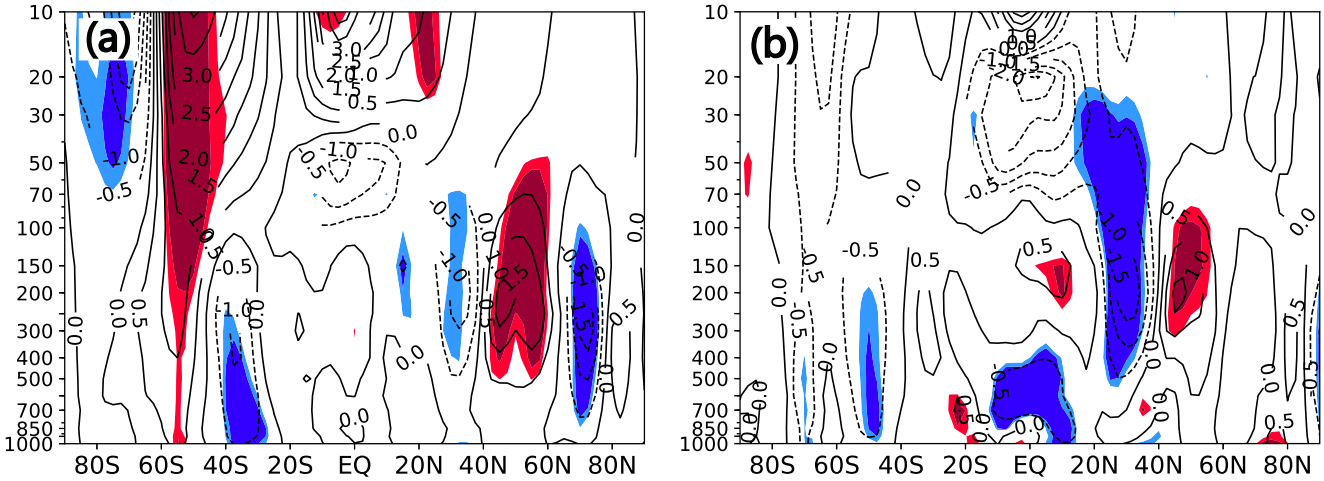

Fig. 5 Latitude-Altitude section for slopes of JA zonal mean (110–120°E) zonal wind with (a) M-AAOI (b) SPNCI (x-axis represents latitude, y-axis represents pressure level, shaded: same as Fig. 1b)

(same longitude, but latitude from 40°N to 45°N) and SSI was not significant (Figures not shown).

In addition, we used the daily long-term means (1981–2010) reanalysis data of heat flux and sea ice concentration to draw the intra-seasonal variations of SSI and HFI (Including index for KA1, KA2 and composite difference between KA1 and KA2). It was found that in the beginning of August, the HFI shows a decreasing trend even though it keeps positive phase (Figures not shown). The correlation coefficients between the SSI and HFI of each key area (KA1

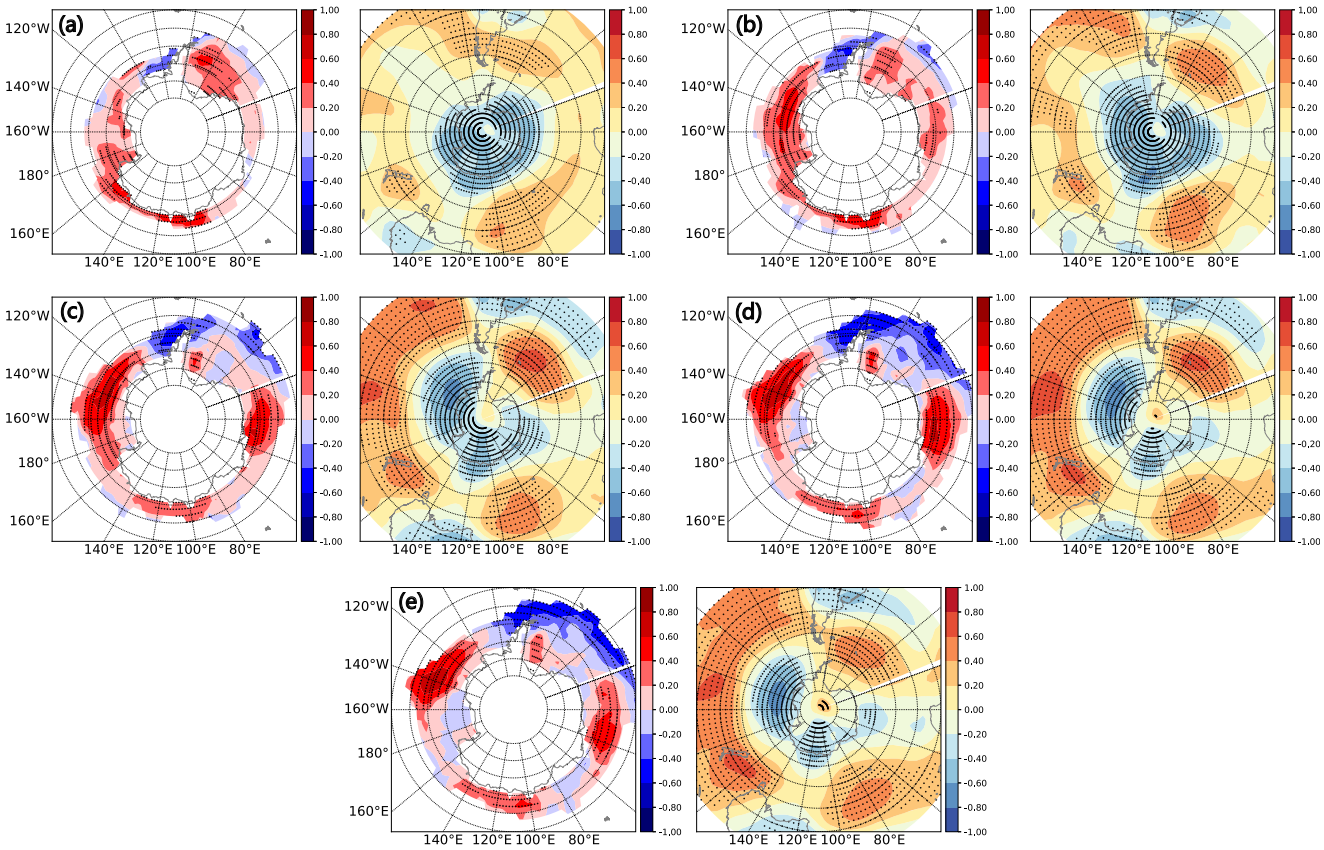

Fig. 6 Leading MCA pattern of heterogeneous correlation field between JA-ASIC and H700 on (a) MA (b) AM (c) MJ (d) JJ (e) JA for 1979 to 2014 (The one on the left hand side is the heterogeneous correlation map of left field, which means the correlation coefficients between time series of right field (H700) and special mode of left field (JA-ASIC). The one on the right hand side is the heterogeneous correlation map of right field. Dotted region denotes such region reaches the statistically significant $p \leq 0.1$)

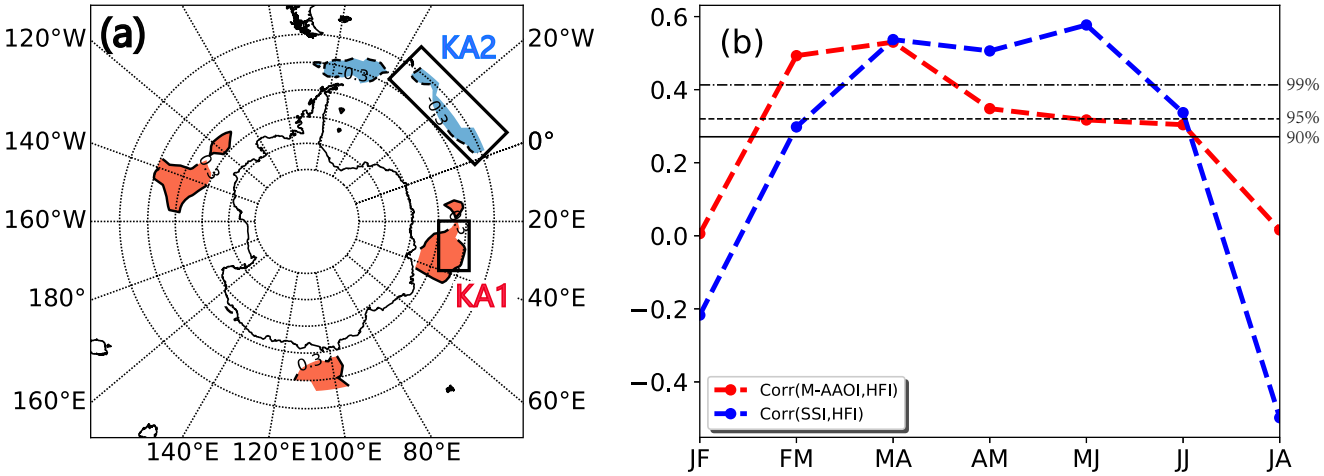

Fig. 7 (a) Correlations between M-AAOI and JA-ASIC (Shaded: reaches the statistically significant $p \leq 0.1$, red: positive, blue: negative) (b) Correlations between M-AAOI, SSI and HFI from JF to JA for 1979 to 2014 (X-axis represents months while Y-axis represents correlation coefficients. Blue dashed line represents correlation plots between M-AAOI and HFI, while red dashed line represents correlation plots between SSI and HFI. Three black lines represent significant confident level of 90%, 95% and 99%, respectively)

and KA2, respectively) from MA to JA (we choose 30 days per month for the calculation) exhibit significant positive from MA to MJ, and negative from JJ to JA, with high values that reached statistically significant $p \leq 0.01$. But the correlation coefficients between composite difference SSI and HFI were negative from MA to JA, and reached the statistically significant $p \leq 0.05$ from MA to MJ and $p \leq 0.01$ from JJ to JA. For daily AAOI, the correlation coefficients between MA-AAOI and MA-HFI of KA1, KA2 are −0.267 and − 0.166 respectively, while the correlation between MA-AAOI and MA-HFI (difference between KA1 and KA2) was relative less. The details are shown in Table 1. Significant negative correlation between boreal spring AAO and HF represents the atmospheric signals imprint into the underlying surface by the heat absorption of underlying surface, persist to the following summer by complex mechanisms (Wu and Zhang, 2011; Hu et al. 2016; Xiao et al. 2016). For the relatively higher values in the 4th and 5th rows of Table 1, the process of atmospheric signals storing and releasing through the heat exchanging is represented.

3.2 Impact of Antarctic Sea Ice on North China Precipitation

Results from routine examination show that, in the year of high SSI, whenever the subtropical high is west, the Australia high is strengthened. This is similar with the results from previous studies (Xue et al. 2003; Gao et al. 2003; Ho et al. 2005) which have pointed out that western subtropical high and strengthening of Australia high could lead in a wave trend as Japan-Pacific, which will further affect summer precipitation in China.

Figure 8a, b show meridional circulation anomalies of high and low SSI years and Fig. 8c shows the composite difference of meridional circulation between high and low SSI years. The shading of these figures represents the climatology pattern of summer vertical velocity, same as Fig. 4. Ascending anomalies over 35°N to 40°N are observed in the high SSI years (Fig. 8a) while descending anomalies over 35°N to 40°N and ascending anomalies moving northward in the low SSI years (Fig. 8b). From composite difference meridional profile (Fig.

Table 1 Correlation coefficients between MA-AAOI, SSI and HFI from JF to JA

Key Areas		MA-HFI	AM-HFI	MJ-HFI	JJ-HFI	JA-HFI
MA-AAOI	KA1	−0.267**	0.019	–	–	–
	KA2	−0.166	−0.150	–	–	–
	KA (Composite)	−0.040	0.167	–	–	–
SSI	KA1	0.843***	0.695***	0.314**	−0.217*	−0.755***
	KA2	0.791***	0.766***	0.675***	−0.652**	−0.376***
	KA (Composite)	−0.278**	−0.228*	−0.268**	−0.525***	−0.618***

The correlation coefficient with * means the value reaches the statistically significant $p \leq 0.1$ (while ** $p \leq 0.05$; *** $p \leq 0.01$); '–' represents the correlation coefficient is too low

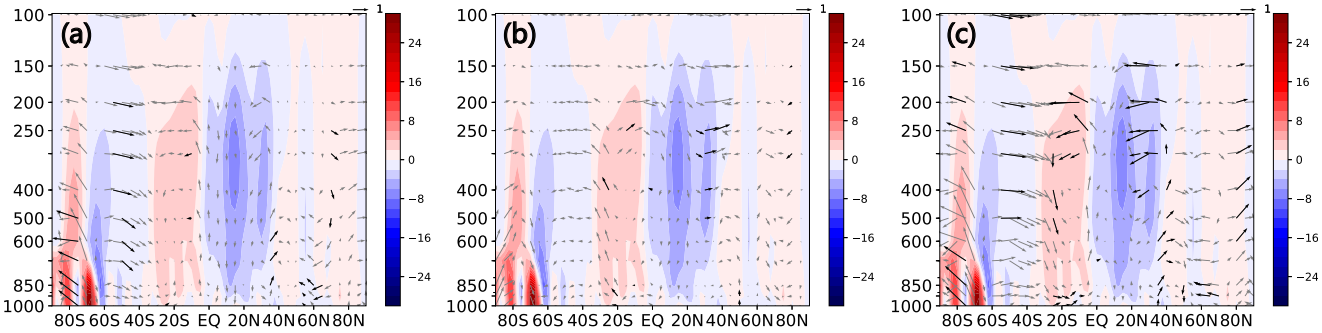

Fig. 8 JA Meridional circulation anomalies for the years of (a) high SSI (b) low SSI; (c) Composite difference of JA meridional circulation between high and low SSI years. (Shaded: Climatology vertical velocity - omega, the unit of omega: 1% Pa/s; Black vector: composite difference reaches the 90% confident level for student-t test)

8c), it can be concluded that significant ascending-southerly anomalies exhibit over 35°N to nearly 45°N in high SSI years, consistent with what was shown in Fig. 4 Hence, the SSI-related ascending anomalies partially explain the ascending-southerly anomalies associated with March AAO in southern part of North China (Fig. 4).

We calculated the T-N flux (W) to clarify the physical mechanism. Figure 9a shows the composite difference of JA horizontal components of T-N flux ($W_{x\text{-}y}$) and JA Perturbation Stream Function (PSI) at 200 hPa between high and low SSI years (The figures for the W and PSI anomalies of high and low SSI years not shown). In the SH, the wave source is located over the Southeast Pacific, with the wave train propagates eastward. In the NH, the wave source is located over the East Asia-Siberia and west Pacific, with the significant dipole PSI anomalies region. It also exhibits the polar-vortex anomaly caused by the anomalous PSI with the southeastern propagation of Rossby waves. The PSI anomalies also exhibit a dipole structure over the East Asia and Siberia, consistent with what had been shown on Fig. 5. From the vertical profiles of composite difference of zonal mean $W_{y\text{-}p}$ and PSI ([$W_{y\text{-}p}$] and [PSI]) between high and low SSI years (Fig. 9b), we found that the planetary wave flux in the SH extratropical exhibited northerly-ascending anomaly accompanied with the anomalous variability of [PSI] from the mid-troposphere to the stratosphere existed over the polar region in the high SSI years compared to that in the low SSI years. Wave-current interaction leads the weakening of descending motion of the stratosphere and the troposphere at high latitude, and the strengthening of circumpolar westerly. Such variabilities in zonal, meridional and vertical wind corresponded to the deepening of Antarctic polar vortex. Meanwhile, the composite difference of the low latitude stratospheric [PSI] which is corresponded to the westerly anomaly of the low latitude stratosphere shows out of phase with that of the Antarctic [PSI], between the high and low SSI years.

In the vertical profiles of zonal mean (20–30°E, 5–40°W in the SH and 110–120°E in the NH) T-N flux ($W_{y\text{-}p}$) and PSI anomaly (Fig. 10a to c), we found that Rossby wave propagates upward to the stratosphere from SH mid-latitudes (Over the KA1 and KA2, the values of $W_{y\text{-}p}$ are extremely high), PSI anomalies occur in the upper and middle troposphere and stratosphere over the high latitude to polar region in the SH. Especially from Fig. 10c, PSI anomalies also occur over North China which shows the center at 200 hPa, in phase with the PSI anomaly in the equatorial stratosphere, corresponding with Fig. 5. The anomalous wave-current interaction over 35 to 50°N is represented by downward-northward propagation

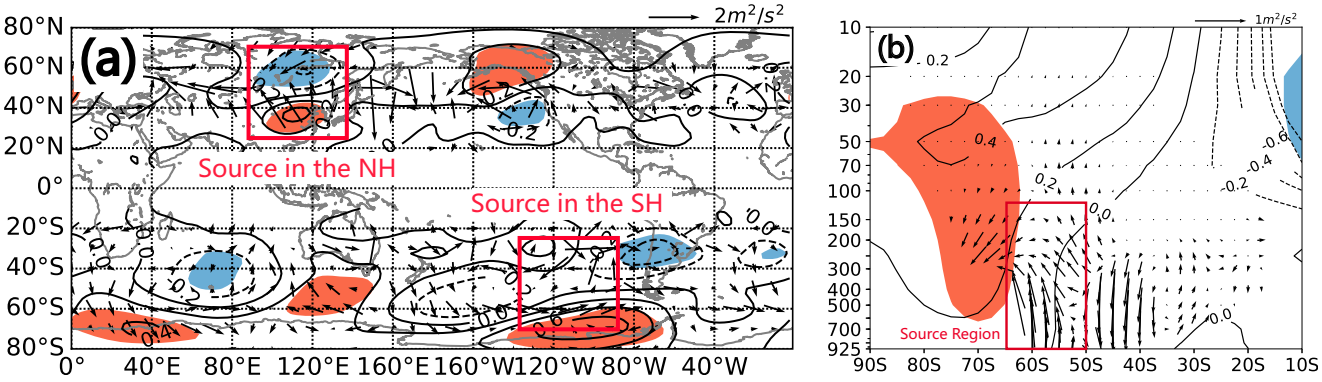

Fig. 9 Composite difference of JA $W_{x\text{-}y}$, $W_{y\text{-}p}$ vectors and PSI values between high and low SSI years (a) Horizontal section of 200 hPa (b) Latitude-Altitude section of zonal mean in the SH (Shading: confidence level reaches 90% for student-t test of the PSI anomalies; Vectors: W vectors; Contours: PSI anomalies; Values of PSI are reduced by 100 times; Values of W_p are expanded by 300 times)

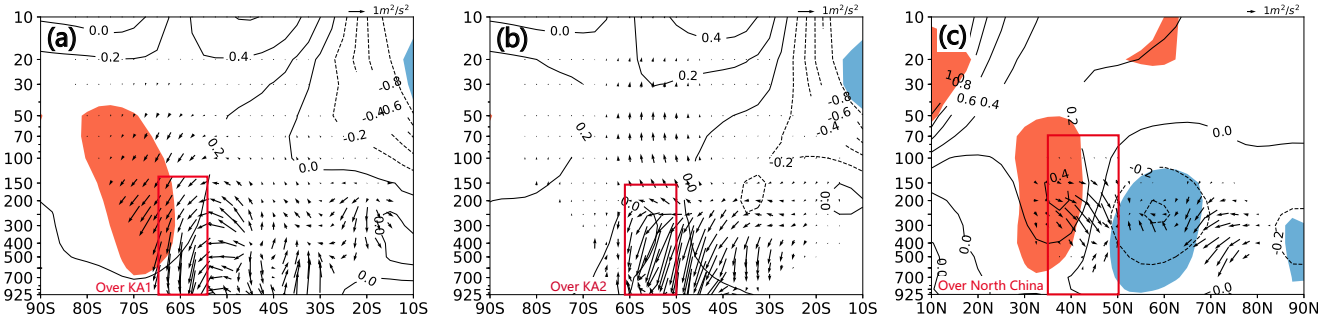

Fig. 10 Composite difference of JA $W_{y\text{-}p}$ vectors and PSI values between high and low SSI years: Latitude-Altitude section of (a) 20–30°E in the SH (b) 5–40°W in the SH (c) 110–120°E in the NH (Same as Fig. 9)

of Rossby waves which can lead to the enhancement of ascending motion and westerly wind over the corresponding region. It is beneficial to SPNC and vice versa.

3.3 The Possible Influence of Stratospheric Zonal Wind on ASIC and SPNC

The main modes of summer zonal mean spatial field, the first mode (EOF1) is obtained throμgh EOF decomposition of JA zonal mean (110–120°E) zonal wind, as shown in Fig. 11. QBO is a quasi-periodic variation phenomenon of the lower stratospheric wind field near the equator, which was discovered in the 1960s (Baldwin et al. 2001). QBO has been found to have impacts on NH climate such as precipitation anomalies by adjusting Indian monsoon and the zonal wind anomaly over the west Pacific (Ho et al. 2009; Coy et al. 2017; Varotsos et al. 2017; Zhang et al. 2017). It was found that the correlation coefficient between PC1 (Time series for EOF1 spatial field) and SSI was equal to 0.283, reached statistically significant $p \leq 0.1$. We also found that JA-QBOI was highly related to PC1, the correlation coefficient was equal to 0.827. In the following analysis, we regard PC1 as QBOI. In addition, the formation of rainy season in the North China is complicated and QBO is not the only influencing factor, since the correlation between QBOI and SPNCI was not significant. It is sμggested that QBO may operate as conduit which connects

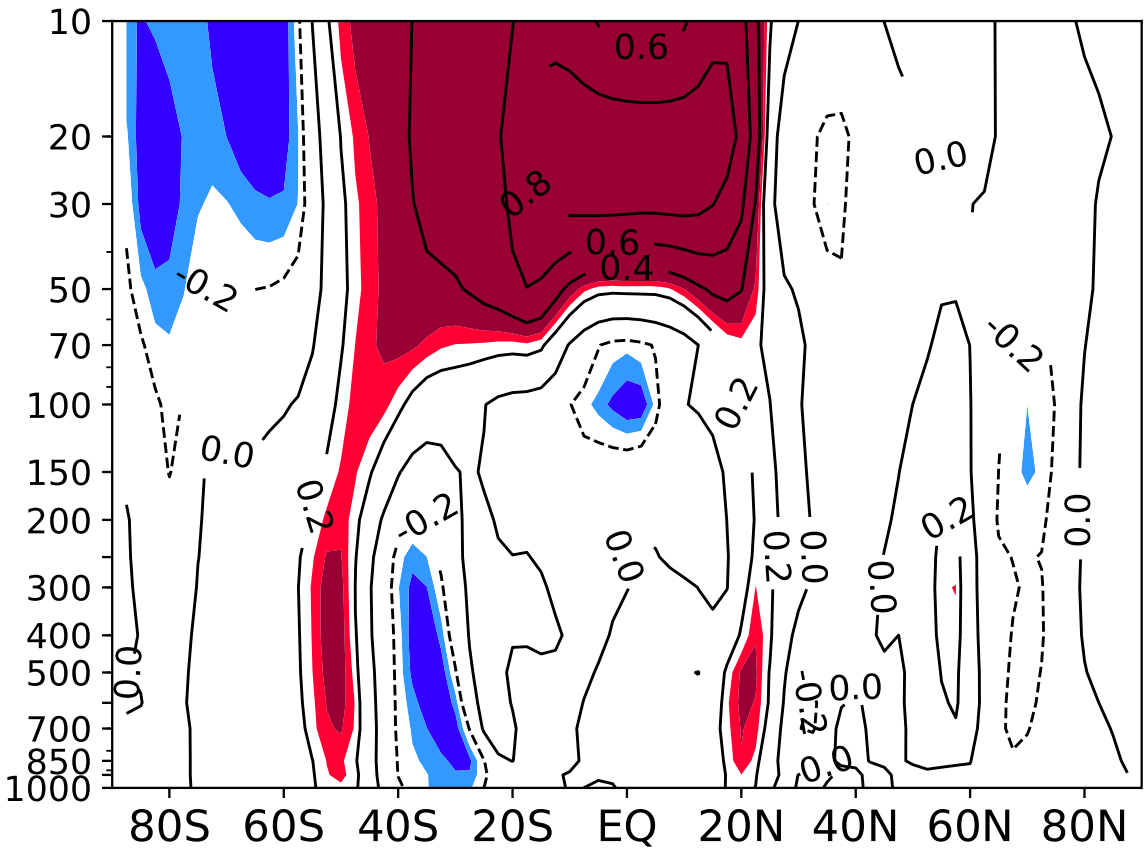

Fig. 11 Latitude-Altitude section of EOF1 of JA zonal mean (110–120°E) zonal wind (Same as Fig. 5)

the summer SSI and zonal wind anomalies in the NH. Through analysis, we find out that in the years of JA QBO easterly phase, zonal wind at 850 hPa exists easterly anomaly in the area of West Pacific at the mid-latitude which benefits SPNC (Figure not show). From Table 2, the correlation coefficient between SSI (with QBOI removed) and SPNCI is higher than that between SSI (with QBOI retained) and SPNCI.

Figure 12a, b show the relationship between SSI (with QBOI removed and retained) and summer zonal mean (110–120°E) zonal wind. Figure 12a represents a significant positive phase from 100 hPa to 10 hPa over the equator from 20°S to 20°N which features a QBO westerly phase corresponding to the increase of SSI. After removing the signal of QBO (Fig. 12b), the westerly anomalies from 50 hPa to 10 hPa over the tropical and subtropical regions have disappeared, the dipole structure exhibits more significant with the signal of QBOI removed than that with QBOI retained, stretches from 500 hPa to 50 hPa with the center of anomalous region at 200 hPa. Note that, the center of zonal wind anomalies in the NH from 20°N to 60°N is at about 200 hPa. From the statistical point of view, the QBO westerly phase may be negative correlated with SPNCI.

To examine the correlation between Antarctic sea ice, QBO and the dipole structure over East Asia, the NCAR Community Atmosphere Model version 5 (CAM5) was used. The horizontal resolution used was 0.9 × 1.25, with 26 hybrid vertical levels (Results were interpolated onto 17 pressure levels). A complete description of this model version is available online at http://www.cesm.ucar.edu/models/cesm1.2/cam/docs/ug5_3/ug.html#intro. We designed a pair of the experiments (E-NC) in which the control run was driven by climatological (1982–2001) sea surface temperature (SST) and sea ice concentration (SIC), the sensitive run was driven by climatological SST and SIC (1982–2001, replaced by reanalysis data) with the SIC increased for 0.2 in KA1 and decreased for 0.2 in KA2. The experiment was integrated for 32 years, and outputs from the last 20 years were used for the analysis to reduce the uncertainties in model spinup caused by initial conditions.

Figure 13a shows the slopes of JA [U] with SSI (with QBOI retained), exhibits AAO like pattern and equatorial-stratospheric positive anomalies (QBO westerly phase). Figure 13b shows the composite difference of zonal wind between the sensitive outputs and the control run outputs for the vertical profile. The module results exhibited a significant dipole structure over the longitude from 110°E to 120°E and the latitude from 20°N to 60°N, especially in the stratosphere, partly corresponding to the observational results. Study by Holton and Tan (1980) had pointed out that QBO could be the candidate of a cause of the interhemispheric synchronization, because of its correlation to the stratospheric polar vortex variations. Figure 13c shows the composite difference of [U] between different outputs, it can be seen that the SSI variability leads a significant difference on equatorial-stratospheric zonal wind, partly consistent with observational results (Figs. 9 and 12a) and previous study (Holton and Tan, 1980). It could be said the M-AAOI/SSI is corresponding to QBO and dipole structure over East Asia continent.

To further investigate the linkage between SSI and SPNC, we used composite analysis method for the years of high SSI (HS), low SSI (LS), westerly phase of QBO (QW) and easterly phase of QBO (QE). Note that, the selection of high or low SSI years in this section is based on 0.5 times standard deviation of standardized SSI. If the standardized SSI is higher than 0.5, it is regarded as positive standard deviation for high SSI years, and if it is lower than −0.5, it is regarded as low SSI years. When QBOI greater than zero indicates the westerly phase, and conversely less than zero indicates the easterly phase. The specific years are shown in Table 3. According to Table 3, we separate the specific years into four groups - high SSI westerly QBO (HS-QW), high SSI easterly QBO (HS-QE), low SSI westerly QBO (LS-QW) and low SSI easterly QBO (LS-QE), respectively.

Previous study by Li and Ma (1992) has pointed out that easterly-phase of QBO at 50 hPa has high relationship with extreme flood in southern part of North China. Study by Xu and Qian (2005) has found the intensity of tropical easterly at 100 hPa has sustainable positive relationship with summer rainfall over North China from spring to summer. They further found the distribution of surface temperature weakens the easterly at 100 hPa and also decreases the sea-land heating contrast which makes the south Asia summer monsoon weaken. This results into water vapor transportation from the South Asia monsoon area to the North China to decrease. That is, the rainfall is less than ever over North China in the years of weak easterly at 100 hPa.

Figure 14a to d show precipitation anomalies in the years of HS-QW, HS-QE, LS-QW and LS-QE. Table 4 shows composite difference of SPNC anomalies in the years of high-low SSI and westerly-easterly phase of QBO over the southern part of North China region (110–120°E, 35–40°N) and the northern part (40–45°N). The unit of precipitation is 'mm'. It can be seen that, precipitation in the years of HS-QW is relatively higher than the others especially in the southern part of North China. Similarly, the precipitation in the years of LS-QW is lower than that in the other groups. That is, in the westerly phase of QBO, the higher the SSI, the higher the

Table 2 Correlation between SSI and SPNCI (SSI with the impact of QBOI and without it)

	SSI	QBOI	SSI (with QBOI removed)
SPNCI	0.350*	−0.116	0.409*

The values with * reached statistically significant ($p \leq 0.05$)

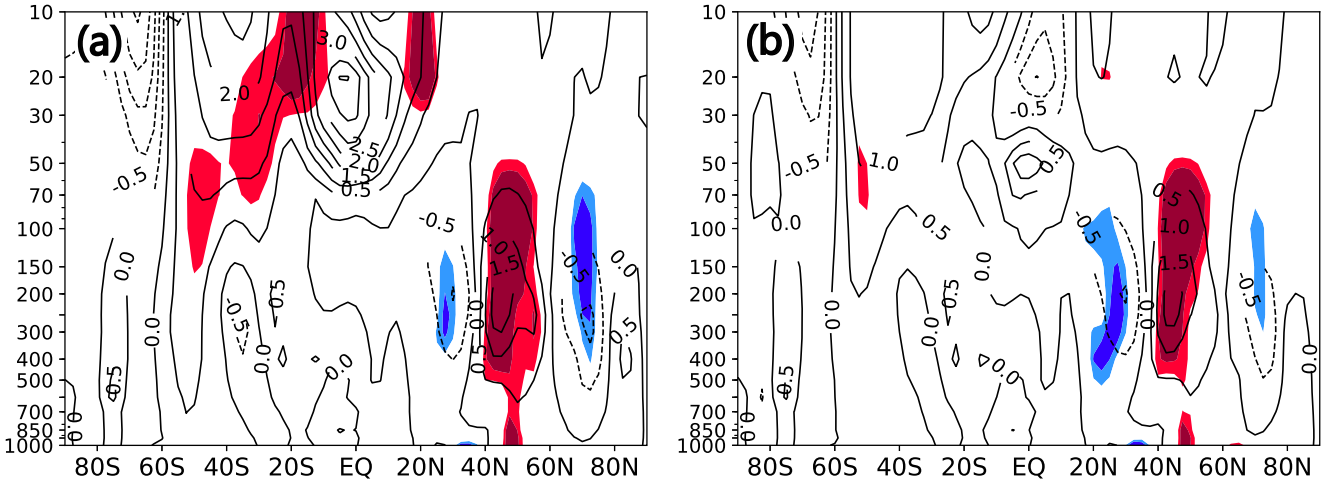

Fig. 12 Latitude-Altitude section for slopes of JA zonal mean (110–120°E) zonal wind with (a) SSI with QBOI retained (b) SSI with QBOI removed (same as Fig. 5)

SPNCI, and vice versa. In the LS-QE years, negative precipitation anomalies region is located in the northern part of North China, but not significantly. For the above analysis, we focus more on HS-QW and LS-QW years. As for composite difference of meridional circulation between HS-QW and LS-QW years (Figures not shown), the significant ascending-southerly anomalies exhibit over 35°N to nearly 45°N in high SSI years, consistent with what was shown in Fig. 8c. Such anomalous meridional-vertical pattern is no longer significant in the years of QBO easterly phase. We also applied the MCA analysis to figure out the relationship between ASIC and SPNC in different phase of QBO. Figure 15a, b show the leading MCA mode between JA-ASIC and JA precipitation in China from 1979 to 2014 in QW and QE, respectively. It could be seen that, the spatial heterogeneous correlation map of the MCA leading pattern shows the East-West dipole pattern of JA-ASIC which is similar to that shown in Fig. 6b to e and Fig. 7a, with the corresponding significant positive precipitation anomalies in the southern part of North China in the QW. However, in the QE, the dipole pattern of JA-ASIC is located westward and northward compared to that in QW. The significant region of JA precipitation anomalies shifts westward and there exist no significant precipitation anomalies in North China.

Figure 16a to d show the averaged $W_{x\text{-}y}$ vectors and PSI anomaly values at 200 hPa for the years of HS-QW, HS-QE, LS-QW and LS-QE, respectively. The SPNC anomalies in the years of HS-QW and LS-QW show the significant positive anomaly and negative anomaly, respectively, exhibit an out of phase characteristic. Similarity, this out of phase characteristic also occurs at 200 hPa for PSI anomalies (Fig. 14a, 16a and 14c, 16c), hence, there exists significant PSI anomalies with Rossby wave propagating eastward during the years of HS-QW and LS-QW. As for QBO easterly phase years, the precipitation anomalies are not that significant over the southern part of North China, consistent with no significant PSI anomalies over such region. In the NH extratropical, the significant Rossby wave train belt over Eurasia continent is moved northward (Fig. 16b, d). Compared to HS-QW years, southern anomalies of Rossby wave train is exhibited in the LS-QW years (Fig. 16a, c). Interestingly, Fig. 4b and 8b show significant descending anomalies for vertical velocity (omega), consistent with the southern anomalies of Rossby wave propagation. From the above analysis, SSI and westerly phase

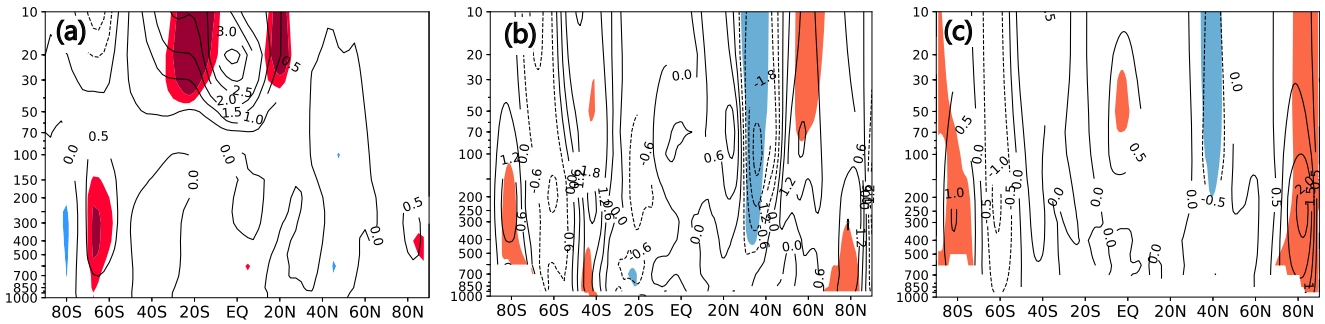

Fig. 13 (a) Latitude-Altitude section for slopes of JA [U] with SSI (with QBOI retained, shaded: same as Fig. 5) (b) Latitude-Altitude section for the composite difference of JA zonal mean (110–120°E) zonal wind for E-NC (c) Latitude-Altitude section for the composite difference of JA [U] for E-NC (Shaded: confidence level reaches 90% for student-t test)

Table 3 Years of high and low SSI and westerly-easterly phase of JA-QBO

	QBO Westerly Phase (QW)	QBO Easterly Phase (QE)
High SSI (HS)	1982, 1990, 1995 2004, 2006, 2010, 2013	1979, 1989, 2003, 2012
Low SSI (LS)	1992, 2002, 1987, 2008	1984, 1998, 2001 2005, 2007, 2011

Time series is from 1979 to 2014, the selection of high or low SSI years is based on 0.5 times standard deviation of SSI

of QBO have significant effects on summer precipitation in the southern part of North China. The similar exhibitions are shown in the vertical profile of HS-QW, HS-QE, LS-QW and LS-QE (Figures not shown).

Figure 17 is the schematic picture for the impact of March AAO on SPNC. It shows the significant influence of preceding AAO on SPNC through cross-season and cross-equator, and highlights the role of QBO westerly phase.

4 Conclusions

Many studies have noticed that the statistical linkage between the AAO and the NH climate, but some of the detailed physical mechanisms remain controversial on how the AAO

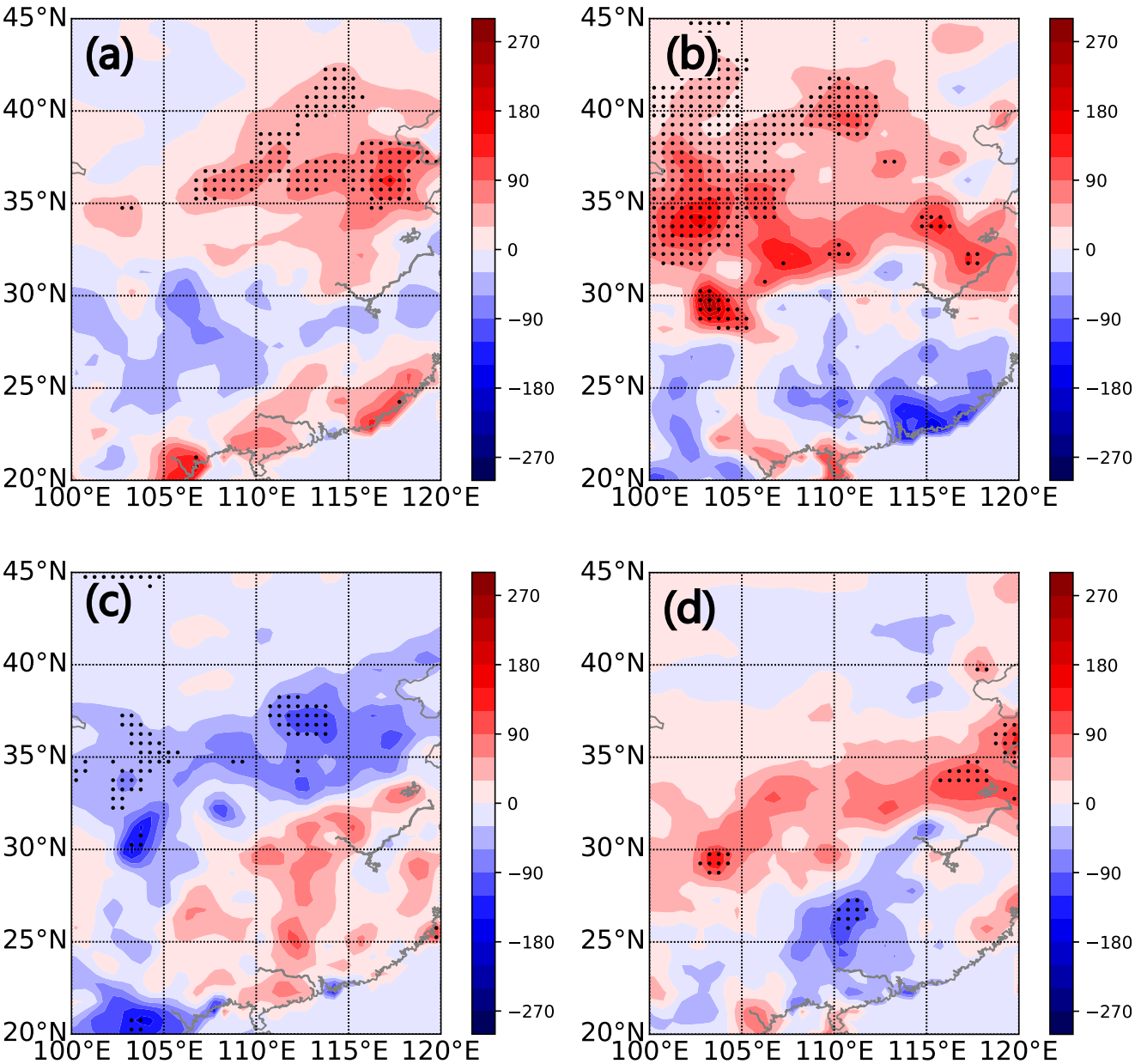

Fig. 14 JA Precipitation anomalies map for the years of (a) HS-QW (b) HS-QE (c) LS-QW (d) LS-QE (Shaded: Precipitation anomalies; Black scatters: reach the 90% confident level for student-t test)

Table 4 SPNC anomalies (90% student t-test significant level) in the years of HS-QW, HS-QE, LS-QW and LS-QE

Mode	HS-QW	HS-QE	LS-QW	LS-QE
Significant Region (90%)	110°E ~ 120°E, 35°N ~ 43°N	110°E ~ 112.5°E, 37.5°N ~ 43°N	110°E ~ 115°E, 35°N ~ 38°N	117.5°E ~ 120°E, 35°N ~ 37.5°N
Composite Difference of Precipitation	30 ~ 120 mm	0 ~ 120 mm	−150 ~ − 60 mm	60 ~ 120 mm

'QW' indicates the westerly-phase, 'QE' indicates the easterly-phase, 'HS' indicates the high SSI, 'LS' indicates the low SSI

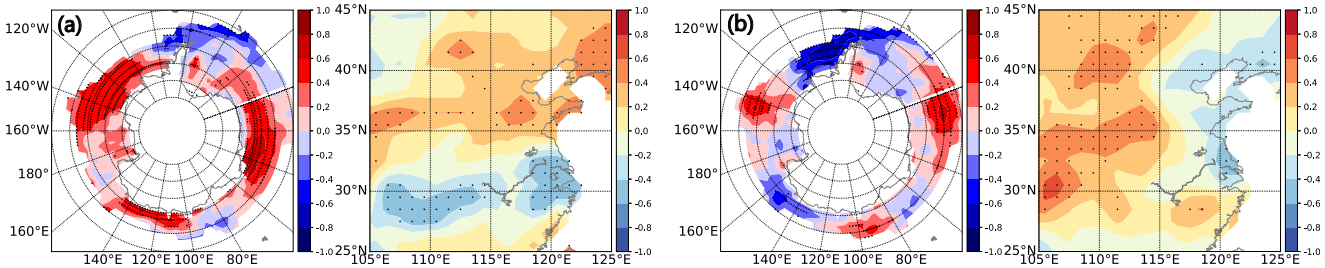

Fig. 15 Leading MCA pattern of heterogeneous correlation field between JA Antarctic sea ice concentration (JA-ASIC) and JA precipitation in China for 1979 to 2014 in (a) QW (b) QE phase (Same as Fig. 6, but the right panel of each subfigure represents JA precipitation in China)

signals propagate from the SH to the NH and further affect the NH climate. This is due to the lack of persistence of atmospheric signals, and how the precursory atmospheric signals are stored in underlying ocean or sea ice and then be released in the following seasons.

This study investigated the effect of spring AAO on SPNC. We conclude that (1) The positive phase of March AAO results in more precipitation in North China in Summer, and vice versa. March AAO uses Antarctic sea ice as a bridge to influence the zonal wind, and meridional circulation in the Northern Hemisphere, resulting in the southeasterly and ascending motion anomalies in the southern part of North China; (2) The pre-stored AAO signals are released from the key areas of Antarctic sea ice, the planetary wave flux propagates upward and poleward by wave-current interaction, resulting in the deepening of polar vortex, the strengthening of circumpolar westerly (AAO like pattern) and the westerly anomalies over the tropical stratosphere (QBO like pattern); (3) In the QBO westerly phase, the SPNC anomaly in the high SSI years shows out of phase with that in the low SSI years.

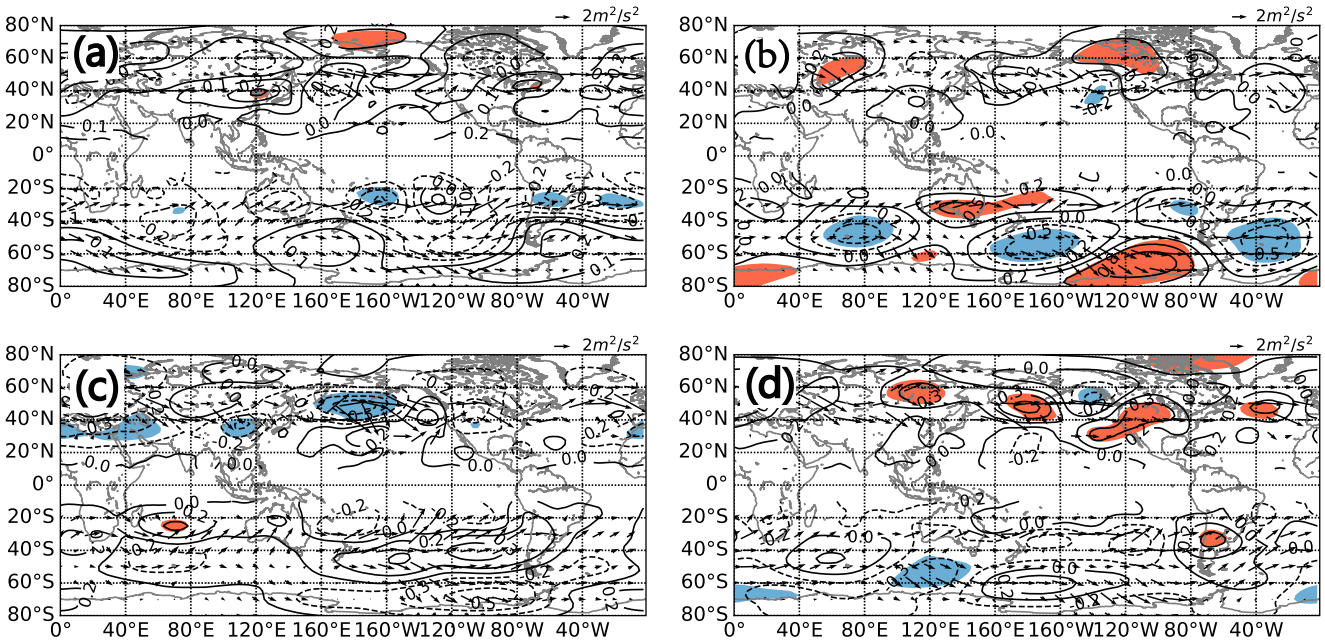

Fig. 16 Averaged JA $W_{x\text{-}y}$ vectors and PSI anomaly values at 200 hPa for the years of (a) HS-QW (b) HS-QE (c) LS-QW (d) LS-QE (Same as Fig. 9)

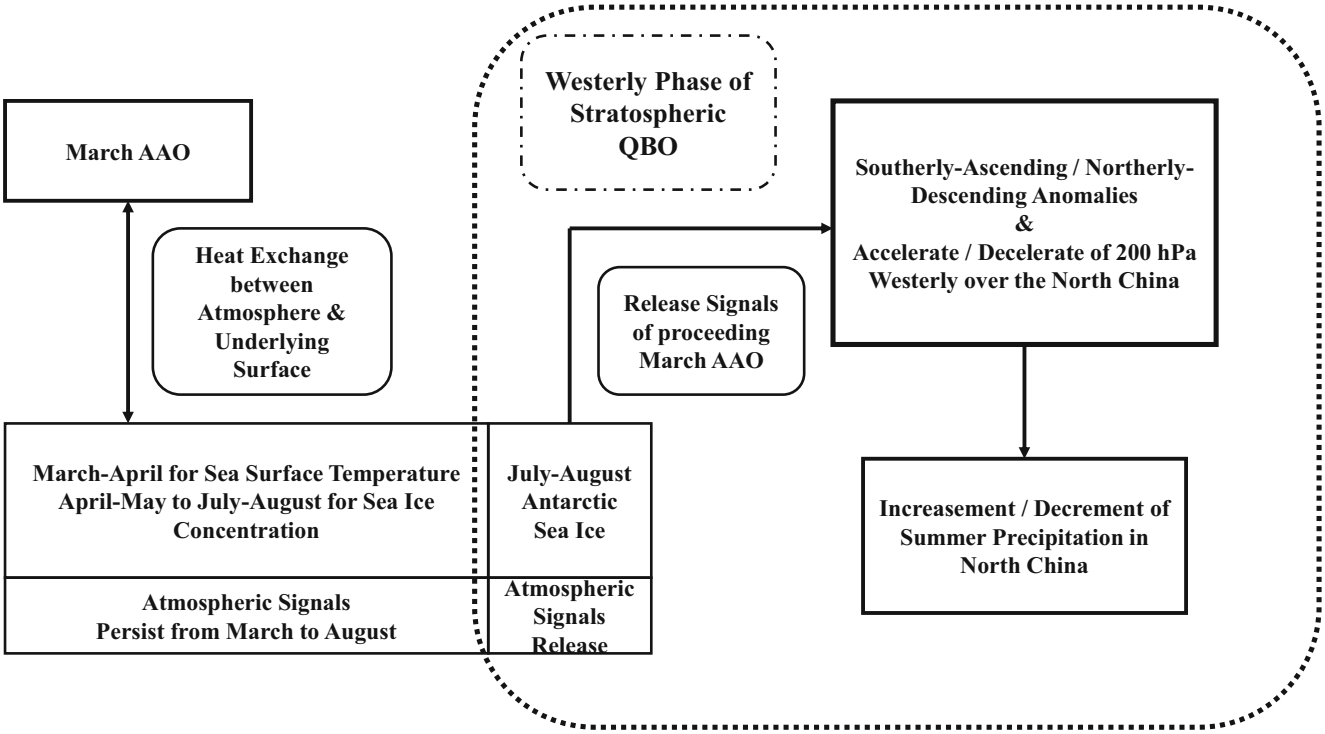

Fig. 17 Schematic picture for the impact of March AAO on SPNC

The SPNC anomalies are significant for student-t test in both high and low SSI years. However, SPNC anomalies are not significant in the QBO easterly phase; (4) There are significant regions of PSI anomaly at 200 hPa over the North China in boreal summer, but the transmission of Rossby wave cannot be found above 100 hPa. There is existence of a region of weak to strong wave energy over North China which is regarded as the source region of wave, accompanied with a significant PSI anomaly in the high and low SSI years of QBO westerly phase. In the years of QBO easterly phase, the PSI does not exhibit at least one significant region which reach the statistically significant, and the significant regions for PSI anomaly and propagation belt of Rossby wave move northward compared with that in the years of QBO westerly phase. Interestingly, Rossby wave has the characteristics of anomalous southward propagation which corresponds to the abnormal weakening of upward motion (the decrease of precipitation) over North China in the low SSI years. The QBO may serve as a 'air bridge' between Antarctic sea ice and NH zonal wind anomalies in summer, the phase of SPNC gives significant anomalies corresponding to the SSI variability in the years of QBO westerly phase.

Based on the findings from this study, there is a need to conduct numerical model experiment to further verify the reliability of the 'ice bridge' and 'air bridge' between AAO and SPNC. The specific mechanism for the formation of stratospheric teleconnection wave train in this study remains to be explored, which is also one of the key tasks in our future research work.

Acknowledgements This study is supported by the Strategic Priority Research Program of the Chinese Academy of Sciences (Grant NO. XDA19070402).

References

Amita, P., Pramod, M., Rambhau, K., Sanjay, B.: Connection between Antarctic Sea-ice extent and indian summer monsoon rainfall. Int. J. Remote Sens. **30**(13), 3485–3494 (2009). https://doi.org/10.1080/01431160802562248

Baldwin, M.P., Gray, L.J., Dunkerton, T.J., Hamilton, K., Haynes, P.H., Randel, W.J., et al.: The quasi-biennial oscillation. Rev. Geophys. **39**(2), 179–229 (2001). https://doi.org/10.1029/1999rg000073

Bian, L., Lin, X.: Antarctica Sea-ice oscillation and its possible impact on monsoon of south sea and China summer rainfall. J. Glaciol. Geocryol. **30**(2), 196–203 (2008). https://doi.org/10.3724/SP.J.1047.2008.00014 (In Chinese)

Bian, L., Lin, X., Xia, L.: Antarctica Sea-ice oscillation and its possible impact on monsoon of south sea. Chinese Journal of Polar Science. **21**(1), 11–21 (2010). https://doi.org/10.3724/SP.J.1085.2010.00011

Bintanja, R., Selten, F.M.: Future increases in arctic precipitation linked to local evaporation and sea-ice retreat. Nature. **509**(7501), 479–482 (2014). https://doi.org/10.1038/nature13259

Choi, K.S., Oh, S.B., Kim, D.W., Byun, H.R.: Possible influence of AAO on north Korean rainfall in august. Int. J. Climatol. **34**(6), 1785–1797 (2014). https://doi.org/10.1002/joc.3801

Coy, L., Newman, P.A., Pawson, S., Lait, L.R.: Dynamics of the disrupted 2015-16 quasi-biennial oscillation. J. Clim. (2017). https://doi.org/10.1175/JCLI-D-16-0663.1

Fan, K., Wang, H.: Antarctic oscillation and the dust weather frequency in North China. Geophys. Res. Lett. **31**(10), 399–420 (2004). https://doi.org/10.1029/2004gl019465

Fan, K.: Atmospheric circulation in southern hemisphere and summer rainfall over Yangtze river valley. Chin. J. Geophys. **49**(3), 599–606 (2006). https://doi.org/10.1002/cjg2.873

Fan, K., Wang, H.: Interannual variability of Antarctic oscillation and its influence on east Asian climate during boreal winter and spring. Science in China. **49**(5), 554–560 (2006). https://doi.org/10.1007/s11430-006-0554-7

Fan, K., Wang, H.: Simulation of the AAO anomaly and its influence on the northern hemispheric circulation in boreal winter and spring. Chin. J. Geophys. **50**(50), 376–382 (2007). https://doi.org/10.1002/cjg2.1045

Gao, H., Xue, F., Wang, H.: Interannual variation of Antarctic oscillation and its impact on Meiyu over the Yangtze-Huaihe River and its forecasting significance. Chin. Sci. Bull. **48**(z1), 87–92 (2003). https://doi.org/10.3321/j.issn:0023-074X.2003.z1.016

Holton, J., Tan, H.: The influence of the equatorial quasi-biennial oscillation on the global circulation at 50mb. J. Atmos. Sci. **37**(10), 2200–2208 (1980). https://doi.org/10.1175/1520-0469(1980)037<2200:TIOTEQ>2.0.CO;2

Huang, R.H. & Li, W.J.: Influence of the heat source anomaly over the tropical western Pacific on the subtropical high over East Asia. Proc. International Conference on the General Circulation of East Asia. 40–51 (1987)

Ho, C.H., Kim, J.H., Kim, H.S., Sui, C.H., Gong, D.Y.: Possible influence of the Antarctic oscillation on tropical cyclone activity in the western north pacific. J. Geophys. Res.-Atmos. **110**(D19), (2005). https://doi.org/10.1029/2005JD005766

Hsu, H.H., Lin, S.M.: Asymmetry of the tripole rainfall pattern during the east Asian summer. J. Clim. **20**(17), 4443–4458 (2007). https://doi.org/10.1175/JCLI4246.1

Ho, C.H., Kim, H.S., Jeong, J.H., Son, S.W.: Influence of stratospheric quasi-biennial oscillation on tropical cyclone tracks in western north pacific. Geophys. Res. Lett. **36**(6), 141–153 (2009). https://doi.org/10.1029/2009GL037163

Hu, C., Wu, Q., Yang, S., Yao, Y., Chan, D., Li, Z., Deng, K.: A linkage observed between austral autumn Antarctic oscillation and preceding Southern Ocean SST anomalies. J. Clim. **29**(6), 2109–2122 (2016). https://doi.org/10.1175/JCLI-D-15-0403.1

He, S., Gao, Y., Furevik, T., Wang, H., Li, F.: Teleconnection between sea ice in the Barents Sea in June and the silk road. Pacific-Japan and East Asian rainfall patterns in August. ADV ATMOS SCI. **35**(1), 52–64 (2018). https://doi.org/10.1007/s00376-017-7029-y

Li, Z., Ma, S.: Relationship between the phase of 50 hPa QBO in summer season and the precipitation in the south of North China. Meteorological Monthly. **18**(9), 3–7 (1992). https://doi.org/10.7519/j.issn.1000-0526.1992.9.001 (In Chinese)

Lin, A., De-Jun, G., Bin, Z., Chun-Hui, L., Zhong-Ping, J.: Relationship between South China Sea summer monsoon onset and Southern Ocean sea surface temperature variation. Chin. J. Geophys. **56**(2), 383–391 (2013). https://doi.org/10.6038/cjg20130203

Liu, T., Li, J., Zheng, F.: Influence of the boreal autumn southern annular mode on winter precipitation over land in the northern hemisphere. J. Clim. **28**(22), (2014). https://doi.org/10.1175/JCLI-D-14-00704.1

Li, Y., Guo, P.: Characteristics and mechanisms of unimodal and bimodal precipitation processes in North China in summer. Trans. Atmos. Sci. **38**(4), 540–548 (2015). https://doi.org/10.13878/j.cnki.dqkxxb.20140918001

Nitta, T.: Convective activities in the tropical Western Pacific and their impact on the northern hemisphere summer circulation. J. Meteorol. Soc. Jpn. **65**, (1987). https://doi.org/10.2151/jmsj1965.65.3_373

Plumb, R.: On the three-dimensional propagation of stationary waves. J. Atmos. Sci. **42**(3), 217–229 (1985). https://doi.org/10.1175/1520-0469(1985)042<0217:OTTDPO>2.0.CO;2

Qin, J., Wang, P., Ye, M., Cui, C.: Impacts of February Antarctic oscillations on summer precipitation in eastern China. Acta Meteorologica Sinica. **18**(3), 363–368 (2004) (In Chinese)

Qin, J., Wang, P.X., Gong, Y.: Impacts of Antarctic oscillation on summer moisture transport and precipitation in eastern China. Chin. Geogr. Sci. **15**(1), 22–28 (2005). https://doi.org/10.1007/s11769-003-0064-x

Silvestri, Gabriel, E.: Antarctic oscillation signal on precipitation anomalies over southeastern South America. Geophys. Res. Lett. **30**(21), 2115 (2003). https://doi.org/10.1029/2003gl018277

Screen, J.A.: Influence of arctic sea ice on European summer precipitation. Environ. Res. Lett. **8**(4), 4015 (2013). https://doi.org/10.1088/1748-9326/8/4/044015

Song, F., Zhou, T.: Interannual variability of east Asian summer monsoon simulated by CMIP3 and CMIP5 AGCMS: skill dependence on Indian ocean–western pacific anticyclone teleconnection. J. Clim. **27**(4), 1679–1697 (2014). https://doi.org/10.1175/JCLI-D-13-00248.1

Song, J., Zhou, W., Li, C., Qi, L.: Signature of the Antarctic oscillation in the northern hemisphere. Meteorog. Atmos. Phys. **105**(1–2), 55–67 (2009). https://doi.org/10.1007/s00703-009-0036-5

Shao, X., Li, S., Liu, N., Song, J.: The madden–Julian oscillation during the 2016 summer and its possible impact on rainfall in China. Int. J. Climatol. **38**(5), (2018). https://doi.org/10.1002/joc.5440

Sun, W., Li, J., Yu, R., Yuan, W.: Circulation structures leading to propagating and non-propagating heavy summer rainfall in central North China. CLIM DYNAM. **7**, 1–19 (2018). https://doi.org/10.1007/s00382-018-4090-x

Thompson, D.W.J., Wallace, J.M.: Annular modes in the extratropical circulation. Part I: month-to-month variability*. J. Clim. **13**(5), 1000–1016 (2000). https://doi.org/10.1175/1520-0442(2000)013<1000:amitec>2.0.co;2

Tu, K., Yan, Z.W., Dong, W.J.: Climatic jumps in precipitation and extremes in drying North China during 1954-2006. J METEOROL SOC JPN. Ser. II. **88**(1), 29–42 (2010). https://doi.org/10.2151/jmsj.2010-103

Tan, G., Chen, H., Sun, Z., Den, W.: Linkage of the cold event in January 2008 over China to the North Atlantic oscillation and stratospheric circulation anomalies. Chin. J. Atmos. Sci. **34**(1), 175–183 (2010)

Takaya, K., Nakamura, H.: A formulation of a phase-independent wave-activity flux for stationary and migratory Quasigeostrophic eddies on a zonally varying basic flow. J. Atmos. Sci. **58**, 608–627 (2001). https://doi.org/10.1175/1520-0469(2001)058<0608:AFOAPI>2.0.CO;2

Varotsos, C.A., Sarlis, N.V., Efstathiou, M.: On the association between the recent episode of the quasi-biennial oscillation and the strong El Niño event. Theor. Appl. Climatol. (2017). https://doi.org/10.1007/s00704-017-2191-9

Wu, L., Liu, Z., Li, C., Sun, Y.: Extratropical control of recent tropical pacific decadal climate variability: a relay teleconnection. CLIM DYNAM. **28**(1), 99–112 (2007). https://doi.org/10.1007/s00382-006-0198-5

Wu, Q.: Associations of diurnal temperature range change with the leading climate variability modes during the northern hemisphere wintertime and their implication on the detection of regional climate trends. J. Geophys. Res.-Atmos. **115**(D19), (2010). https://doi.org/10.1029/2010JD014026

Wu, Q., Zhang, X.: Observed evidence of an impact of the Antarctic Sea ice dipole on the Antarctic oscillation. J. Clim. **24**(16), 4508–4518 (2011). https://doi.org/10.1175/2011JCLI3965.1

Xue, F., Wang, H., He, J.: Interannual variability of Mascarene high and Australian high and their influences on summer rainfall over East Asia. Chin. Sci. Bull. **48**(5), 492–497 (2003). https://doi.org/10.1007/bf03183258

Xu, Z., Qian, Y.: Climatic effects of 100 hPa easterly air flow in tropical (II): its relationship with summer rainfall in North China. Plateau Meteorology. **24**(4), 570–576 (2005). https://doi.org/10.1007/s10409-004-0010-x

Xiao, B., Zhang, Y., Yang, X., Nie, Y.: On the role of extratropical air-sea interaction in the persistence of the southern annular mode. Geophys. Res. Lett. **43**(16), 8806–8814 (2016). https://doi.org/10.1002/2016GL070255

Yang, S., Deng, K., Ting, M., Hu, C.: Advances in research on atmospheric energy propagation and the interactions between different latitudes. J Meteorol Res. **29**, 859–883 (2015). https://doi.org/10.1007/s13351-015-5088-5

Yang, X.Q., Xie, Q., Zhu, Y.M., Sun, X.G., Guo, Y.J.: Decadal-to-interdecadal variability of precipitation in North China and associated atmospheric and oceanic anomaly patterns. Chin. J. Geophys. **48**(4), 789–797 (2005). https://doi.org/10.1111/j.1745-7254.2005.00209.x

Zhou, T., Yu, R.: Sea-surface temperature induced variability of the southern annular mode in an atmospheric general circulation model. Geophys. Res. Lett. **31**(24), L24206 (2004). https://doi.org/10.1029/2004gl021473

Zhang, L., Karnauskas, K.B., Weiss, J.B., Polvani, L.M.: Observational evidence of the downstream impact on tropical rainfall from stratospheric kelvin waves. CLIM DYNAM. (2017). https://doi.org/10.1007/s00382-017-3844-1

Zhao, S., Chen, L., Cui, T.: Effects of ENSO phase-switching on rainy-season precipitation in North China. Chin. J. Atmos. Sci. **41**(4), (2017). https://doi.org/10.3878/j.issn.1006-9895.1701.16226